The Astrophysical Journal, 868:124 (14pp), 2018 December 1 https://doi.org/10.3847/1538-4357/aae92c

Statistical Study of ICMEs with Low Mean Carbon Charge State Plasmas Detected from 1998 to 2011

Xuedong Feng[1,2], Shuo Yao[1], Dongni Li[1], Gang Li[1,3], and Xiaoli Yan[4]
[1] School of Geophysics and Information Technology, China University of Geosciences (Beijing), 29 XueYuan Road, Haidian District, Beijing, 100083, People's Republic of China; yaoshuo@cugb.edu.cn
[2] Key Laboratory of Geospace Environment, Chinese Academy of Sciences (CAS), Hefei, 230026, People's Republic of China
[3] Center of Space Plasma and Aeronomic Research, University of Alabama in Huntsville, Huntsville, AL 35899, USA
[4] Yunnan Observatories, Chinese Academy of Sciences Kunming, 650216, People's Republic of China
Received 2018 January 23; revised 2018 October 14; accepted 2018 October 14; published 2018 November 30

Abstract

We present a statistical study of 219 ICMEs measured by both *ACE* and *WIND* from 1998 to 2011. ICME plasmas are defined as possessing cold materials if the carbon average charge states are lower than those of the preceding solar wind by three standard deviations and the carbon ionic temperature is lower than $10^{6.05}$ K. A total of 69 ICMEs were identified as containing cold materials. These ICMEs tend to have speeds in the range of 300–600 km s^{-1}, with durations between 2 and 6 hr. Cold materials tend to be present once or twice per ICME. We further identify two special types of cold materials: the ionic-cold type (IC) shows simultaneous lower average charge states of O, Mg, Si, and Fe ions than those of the preceding solar wind, while the carbon-only cold type (COC) shows a totally opposite trend in that these ions show higher average charge than in the preceding solar wind. We found that the IC has a higher proton temperature than the ICME mean value, whereas the COC has a lower proton temperature than the ICME mean value, and the COC is most often measured in magnetic cloud. A detailed examination of the IC and the COC material suggests that they are related to solar filaments. Their special mean charge indicates that the filaments are a mixture of coronal and choromospheric materials. Heating and collision processes beyond the carbon freeze-in height are crucial in generating the two distinct types.

Key words: Sun: coronal mass ejections (CMEs) – Sun: filaments, prominences

Supporting material: machine-readable tables

1. Introduction

Coronal mass ejections (CMEs) are some of the most severe explosive phenomena in the heliosphere. They have been routinely observed by coronagraphs since the 1970s (Hundhausen et al. 1984; Schwenn et al. 2006). It is well known that halo CMEs can cause geomagnetic storms. Typically, CMEs have a three-part structure: the bright core, the dark cavity, and the bright front. The bright core is supposed to be the eruptive filament, the dark cavity is the flux rope, and the bright front is where the plasmas pile up (Hudson et al. 2006; Wimmer-Schweingruber et al. 2006; Reeves et al. 2015). When CMEs propagate into the interplanetary space, their counterparts measured in situ are called interplanetary coronal mass ejections (ICMEs; Zurbuchen & Richardson 2006). If ICMEs have enhanced magnetic field strength and smoothly rotating magnetic field, they are classified as magnetic clouds (MCs; Burlaga et al. 1981).

In the past 40 years, researchers have attempted to learn more about plasma features and the acceleration process of CMEs from in situ measurements (Cane & Richardson 2003; Richardson & Cane 2010; Howard 2015a, 2015b; Wood et al. 2016). Many works reported the identification of the plasma pileup and flux rope structures. However, cold and dense filaments have been seldom reported from in situ measurements. Usually, it is believed that the solar filament materials come from the chromosphere (Forbes 2000; Yan et al. 2013, 2016). Such materials should show a lower proton temperature, higher proton density, a higher alpha to proton ratio, and lower charge state ions (Priest 1988). According to these criteria, Schwenn et al. (1980), Wurz et al. (1998), Burlaga et al. (1998), Gloeckler et al. (1999), Gopalswamy et al. (1998), Lepri & Zurbuchen (2010), Yao et al. (2010), and Song et al. (2016) identified over 10 ICME events from 1976 to 2009 that likely contained filament materials. Clearly, this number is far less than the number of observed three-part CMEs (Gopalswamy 2006; McCauley et al. 2015). Recently, Song et al. (2016) and Song et al. (2017) analyzed the average ion charge state of Fe inside the ICMEs and confirmed that some cold materials in the ICMEs may not be related to the prominence in the solar atmosphere. A natural problem that arises from these studies concerns what happens to the prominence/filament during the initiation of the CMEs and what is the nature of the cold material in the ICMEs measured in situ. As an attempt to solve these problems, we perform a statistical analysis of all the ICMEs measured by both the *WIND* and *ACE* spacecraft from 1998 to 2011 with a focus on cold materials. By combining the ion average charge of C, O, Mg, Si, and Fe; proton and α particle moments; and solar observations; we examine the features of the cold materials in the ICMEs. The data and the criteria used to identify the cold materials are described in Section 2. The statistical results of the cold materials in the ICMEs are shown in Section 3. Constraints on possible physical processes as revealed by the presence of these cold materials are discussed in Section 4.

2. Data and Criteria

We used the magnetic field, proton temperature, proton speed, and ion charge state distributions measured by the *ACE*

spacecraft from 1998 to 2011. The magnetic field magnitude and its components in the Geocentric Solar Ecliptic (GSE) coordinate system are provided by the MFI every 16 s (Smith et al. 1998). The normalized ion charge distributions of C, O, Mg, Si, and Fe are published with a cadence of one hour by SWICS (Gloeckler et al. 1998), and the plasma moments are provided with a cadence of 64 s by SWEPAM (McComas et al. 1998). All the ion charge state data is provided by the *ACE* Science Center. To minimize the effect of instrument errors and to help better identify the MC, this work also uses *WIND* data, including the 3 s magnetic field magnitude provided by MFI (Lepping et al. 1995), the 92 s cadence proton density N_p and α particle density N_α provided by SWE (Ogilvie et al. 1995) and the 3 s cadence proton temperature T_p provided by 3DP (Lin et al. 1995). The CME images observed by LASCO and UVCS on board *SOHO* (Dere et al. 1997) available at http://cdaw.gsfc.nasa.gov/CME_list/ are used to analyze the initial structures of the ICMEs detected between 1998 February and 2005 August (Giordano et al. 2013). Since UVCS on board *SOHO* ceased to work in September 2005, *STEREO* is the only spacecraft offering continuous Halo CME observations in which the core part could be clearly identified from 2007 to 2011. After 2007 April, the CME movies observed by SECCHI and EUVI on board *STEREO* available at https://secchi.nrl.navy.mil/cactus are used (Aschwanden et al. 2009).

The ICME list used in this work is given by Cane & Richardson (2003); Richardson & Cane (2010), and by the *ACE* Science Center http://www.srl.caltech.edu/ACE/ASC/DATA/level3. Of all 319 ICME events from 1998 February to 2011 August, when the SWICS data is available, 219 events were detected by both the *WIND* and *ACE* spacecraft, together with the 24 hr of solar wind before them. For this analysis, we required data gaps in the ionic charge states to be shorter than 12 hr in the preceding solar wind and 2 hr in ICME periods, as well as shorter than 6 times the sampling cadence for other plasma parameters. The detailed ICME event list is shown in Table 6 in the Appendix. All the times of the shock and ICME leading and trailing edges are shown with respect to *ACE* time. The shock time is used to determine the 24 hr solar wind preceding the ICME. The mean value of all the statistics is calculated from the ICME leading edge to trailing edge. To examine whether the ICMEs are MCs, we used the criterion given by Burlaga et al. (1981). Specifically, an ICME is identified as an MC if the magnetic field magnitude is enhanced stably and the magnetic field vector rotates smoothly for a large angle. To avoid subjective judgment, we quantified the criterion as follows: the maximum magnetic field magnitude of the ICME is stronger than that of the ICME sheath, the elevation angle of the magnetic field changes by at least 50° over more than 8 hr, and the fluctuations of the magnetic field elevation angle θ are less than 50% of the $\theta_{max} - \theta_{min}$ in the ICME.

In all analyzed 219 ICME events, there are 99 MCs. Since we focused on the nature of the cold materials in the ICMEs, we analyzed not only the ion charge state but also the proton temperature T_p, the proton density N_p, the proton velocity V_p, the alpha particle density N_α, and the alpha to proton density ratio, $R_{\alpha p} \doteq N_\alpha/N_p$, in the ICMEs and in the preceding 24 hr of solar wind.

The carbon ions have a freezing in height between 1 and 1.2 R_s, which is lower than that of the O, Mg, Si, and Fe ions (Geiss et al. 1995; Kocher et al. 2017). Consequently, the charge of the carbon ions is the least affected by the heating and collisions associated with the CME initiation. We used the following two criteria to identify cold material in ICMEs. (1) The mean carbon charge state in the carbon-cold (CC) period is at least three standard deviations lower than that of the 24 hr solar wind preceding the ICME. The standard deviation is calculated in the preceding 24 hr of solar wind. (2) The carbon ionic temperature satisfies $T_C < T_{crit} = 10^{6.05}$ K. This critical temperature was derived by binning all preceding solar wind periods into six velocity bins with 50 km s^{-1} bin widths centered around 325–575 km s^{-1} and one bin for $v > 600$ km s^{-1}. We then calculated the expected mean carbon ionic temperature according to the statistical relation between solar wind speed and carbon freeze-in temperature given in Kasper et al. (2012). For the solar wind periods with speeds exceeding 600 km s^{-1}, we used $T_C = 10^{5.988}$ K as given by Landi et al. (2014) who analyzed fast ($v > 500$ km s^{-1}) solar wind measured by *Ulysses* from 1994 to 1998 (Gloeckler & Geiss 2007). We computed the weighted average of these temperatures using the number of occurrences per velocity bin as weights and found $T_{crit} = 10^{6.05}$ K. The ionic temperatures were derived from their mean charge state (as provided by the *ACE* Science Center) using the CHIANTI database version 8 (Dere et al. 1997; Del Zanna et al. 2015). Because ICMEs can follow each other with less than 24 hr separation, we used the 24 hr of solar wind preceding the first ICME if multiple ICMEs occur. The criterion can be expressed as $\langle Q\rangle_C < \langle Q\rangle_{C,SW}$-$3\sigma_{Q_{C,SW}}$ and $T_C < 10^{6.05}$ K. In addition, this ionic temperature corresponds to a mean carbon charge of 5.1336. The symbol σ is the charge state standard deviation of the 24 hr solar wind preceding the ICME. To avoid errors and uncertainties from charge state measurements, a single data point meeting the criteria was not considered in this work. Consequently, we considered a time period containing at least two SWICS data points, which is at least one hour long in between.

3. Statistical Results

We identified 108 segments in 69 ICMEs that contain CC material. Of the 69 ICMEs, 38 are MCs. We also examined the mean charge states of the O, Mg, Si, and Fe ions in the time periods containing cold material. The ionic temperature of C, O, Mg, Si, and Fe ions of the 108 CC segments are shown in Table 7 in the Appendix. It is very interesting that there are two extreme cases. The first one has mean charge states of all the O, Mg, Si, and Fe ions that are lower than those in the preceding 24 hr of solar wind. The other one has mean charge states of all the O, Mg, Si, and Fe ions that are 3σ higher than those in the preceding 24 hr of solar wind. We named the first case ionic-cold (IC) material and the other case carbon-only cold (COC) material. Among all the 108 CC segments, we classified 6 segments as IC and 15 segments as COC. An ICME containing IC material is shown as an example in Figure 1. From the figure, we can see that the carbon mean charge state falls below the $\langle Q\rangle_{C,SW} - 3\sigma_{Q_{C,SW}}$ at approximately 05:30 UT on 2006 April 14. The low mean charge state lasts for approximately 7 hr and is marked by the blue transparent stripe. In the low carbon charge state period, $\langle Q\rangle_O$, $\langle Q\rangle_{Mg}$, $\langle Q\rangle_{Si}$, and $\langle Q\rangle_{Fe}$ are lower than their mean values in the preceding 24 hr of solar wind. Furthermore, the proton temperature measured by both the *ACE* and *WIND* is higher than the mean value of the ICME. Of the six IC segments, five have a higher proton temperature, similar to that shown in Figure 1.

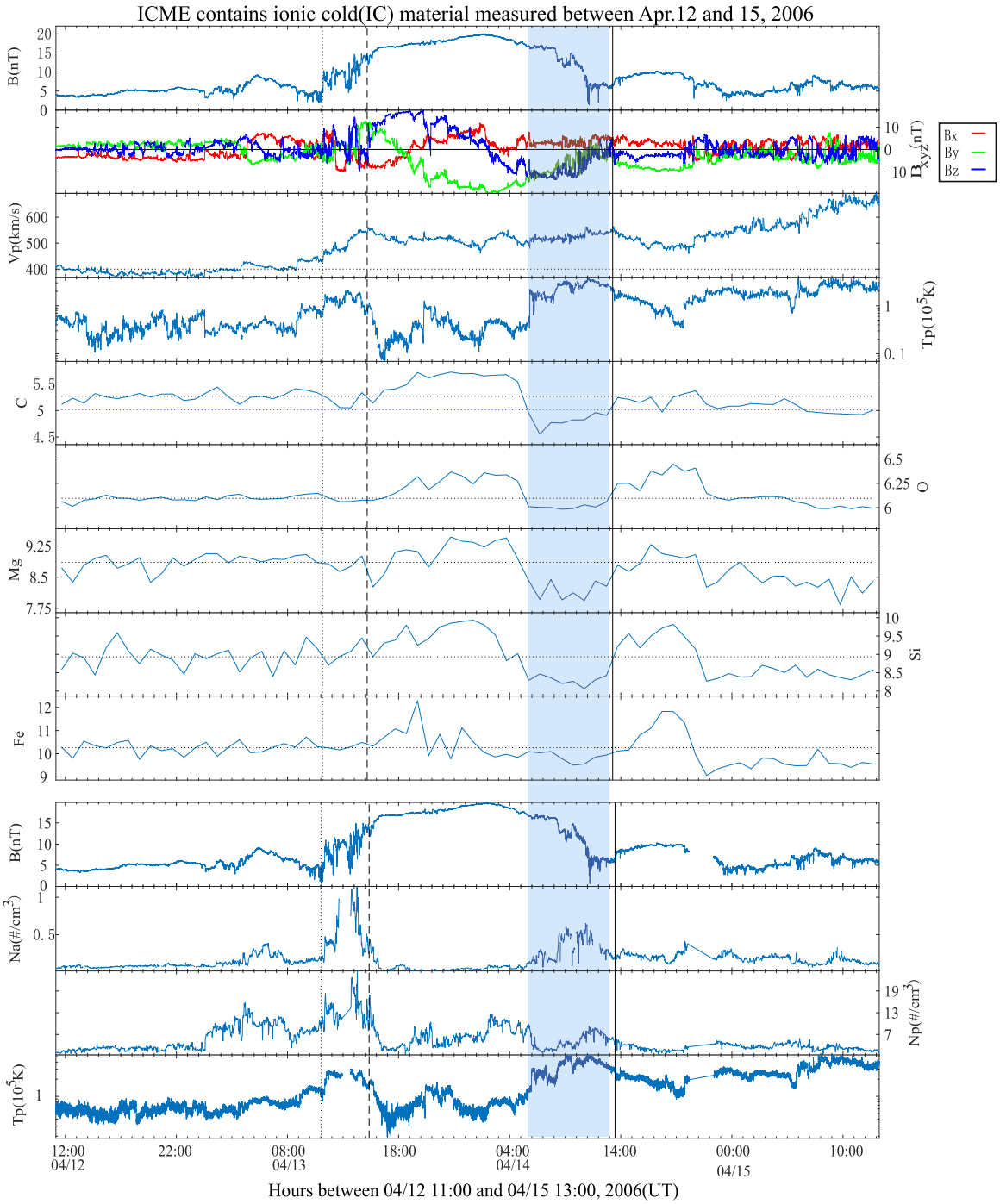

Figure 1. One ICME event containing the IC material. The top nine panels show the magnetic field magnitude, magnetic field components in GSE coordinates, proton speed, proton temperature, $\langle Q\rangle_{\rm C}$, $\langle Q\rangle_{\rm O}$, $\langle Q\rangle_{\rm Mg}$, $\langle Q\rangle_{\rm Si}$, and $\langle Q\rangle_{\rm Fe}$ measured by *ACE*. The remaining four panels display the magnetic field magnitude, α particle density, proton density, and proton temperature measured by WIND. The vertical dotted line denotes the shock in front of the ICME. The vertical dashed line denotes the leading edge of the ICME plasmas. The vertical black solid line denotes the end of the ICME. The horizontal black dotted lines denote the mean charge of ions in the 24 hr of preceding solar wind. In the fifth panel, the horizontal blue dotted line denotes the mean charge of carbon minus three standard deviations. The cold material segment is indicated by the shaded blue stripe.

In Table 1, the six IC segments from five ICMEs are shown with their start and end times, duration, MC or not, and the mean charge state of the C, O, Mg, Si, and Fe ions in the CC segments and in the preceding solar wind. Only one IC period was observed to be inside an MC.

One ICME event containing COC material is shown in Figure 2. From the figure, we can see that the mean carbon charge falls below the $\langle Q\rangle_{\rm C,SW} - 3\sigma_{Q_{\rm C,\,SW}}$ at approximately 07:00 UT on 2000 November 7. The carbon low charge state lasts for approximately 2 hr. During this time, the mean charge states of the O, Mg, Si, and Fe ions are all above their solar wind mean charge state plus three standard deviations of the preceding 24 hr solar wind. Meanwhile, the mean proton temperature measured by *ACE* and *WIND* is lower than that of the CC ICMEs. All of the 15 COC segments except one have a mean $T_{\rm p}$ lower than that of the ICME. All 15 COC segments

Table 1
Ionic-cold Materials in the ICMEs

SN	CC Start (YYYY/MM/DD UT)	CC End (MM/DD UT)	DU	MC	$Q_{C,CC}$	$Q_{C,SW}$	$Q_{O,CC}$	$Q_{O,SW}$	$Q_{Mg,CC}$	$Q_{Mg,SW}$	$Q_{Si,CC}$	$Q_{Si,SW}$	$Q_{Fe,CC}$	$Q_{Fe,SW}$
53	2000 Jun 13 2312	06/14 0431	5^h18^m	No	4.88	5.10	6.23	6.68	9.26	9.36	9.41	9.81	10.03	11.28
191	2006 Apr 14 0538	04/14 1301	7^h23^m	Yes	4.82	5.02	6.01	6.10	8.19	8.86	8.30	8.93	9.86	10.26
201	2009 Jan 19 0542	01/19 1053	5^h10^m	No	4.48	4.60	5.97	6.05	7.76	8.50	7.75	8.68	8.89	9.29
213	2011 Feb 04 2044	02/05 0420	7^h35^m	No	4.75	4.87	6.00	6.13	8.17	8.64	8.29	9.18	9.67	9.93
219	2011 Aug 07 0026	08/07 0248	2^h22^m	No	4.91	4.97	6.10	6.26	8.27	9.26	8.73	9.74	9.81	10.63
219	2011 Aug 07 1824	08/07 2014	1^h49^m	No	4.93	4.97	6.08	6.26	8.57	9.26	8.51	9.74	10.03	10.63

Table 2
Carbon-only Cold (COC) Materials in the ICMEs

SN	CC Start (YYYY/MM/DD UT)	CC End (MM/DD UT)	DU	MC	$Q_{C,CC}$	$Q_{C,SW}$	$Q_{O,CC}$	$Q_{O,SW}$	$Q_{Mg,CC}$	$Q_{Mg,SW}$	$Q_{Si,CC}$	$Q_{Si,SW}$	$Q_{Fe,CC}$	$Q_{Fe,SW}$
13	1998 Sep 25 1432	09/25 1808	3^h36^m	Yes	4.55	4.71	6.34	6.12	9.79	9.20	10.61	8.97	13.97	10.27
17	1998 Nov 09 0408	11/09 0633	2^h25^m	Yes	4.91	4.99	6.25	6.22	9.44	9.26	10.10	9.23	11.95	9.88
24	1999 Apr 16 2158	04/17 1600	18^h1^m	Yes	4.88	5.02	6.35	6.19	9.37	9.04	10.34	9.12	12.17	10.11
31	1999 Jul 28 1947	07/29 0130	5^h43^m	No	4.90	4.99	6.43	6.14	9.47	9.38	10.45	9.28	12.03	9.88
46	2000 Feb 21 1242	02/21 1438	1^h55^m	Yes	5.05	5.14	6.58	6.21	9.54	9.40	11.05	9.45	14.75	10.04
46	2000 Feb 21 2110	02/22 0027	3^h16^m	Yes	4.98	5.14	6.47	6.21	9.61	9.40	10.87	9.45	15.46	10.04
68	2000 Nov 07 0709	11/07 0918	2^h8^m	Yes	4.95	4.97	6.48	6.12	9.61	9.36	10.50	9.36	13.87	10.72
82	2001 Apr 12 1030	04/12 1151	1^h21^m	Yes	4.97	5.01	6.46	6.11	9.65	9.25	11.14	8.79	15.54	9.92
87	2001 Apr 29 0410	04/29 1154	7^h44^m	Yes	4.99	5.11	6.70	6.36	9.91	9.58	11.36	9.91	15.70	11.54
120	2002 Mar 24 1442	03/24 1654	2^h12^m	Yes	5.06	5.18	6.70	6.25	9.79	9.61	11.40	9.56	14.83	10.73
136	2002 Dec 18 0657	12/18 0947	2^h50^m	No	4.96	5.05	6.57	6.30	9.63	9.41	10.77	9.83	12.36	11.35
149	2003 Nov 21 0209	11/21 0354	1^h44^m	Yes	4.91	5.03	6.20	6.15	9.35	9.32	10.07	9.55	12.43	11.31
152	2004 Apr 04 1113	04/04 2251	11^h37^m	Yes	4.95	5.06	6.51	6.16	9.66	9.45	10.99	9.44	13.70	11.17
152	2004 Apr 05 0043	04/05 1102	10^h18^m	Yes	4.90	5.06	6.52	6.16	9.65	9.45	10.71	9.44	12.96	11.17
170	2005 May 15 1519	05/15 1849	3^h29^m	Yes	5.01	5.18	6.76	6.39	9.99	9.80	11.49	10.58	15.54	11.38

from 13 ICMEs are listed in Table 2. It is remarkable that 13 of the 15 COC time periods are identified inside 11 MCs.

Next, we examined various statistics of the 108 CC segments in Figure 3. The histograms of the segments numbers per ICME, of the duration of the segment, and of the proton speed in each segment are plotted. From panel (a), we can see from the figure that most of ICMEs contain one or two cold segments. Only a few of them have more than two segments. The largest number of segments in one ICME is five. Panel (b) shows the distribution of the duration of segments. The most probable value of the duration is 2 hr and most periods are shorter than 10 hr. Nevertheless, there are a few periods that are as long as 37 hr. Panel (c) shows that the bulk solar wind speed in the CC segments lies predominantly between 300 and 600 km s^{-1}, although there are a few faster segments.

Furthermore, we plotted the ratio of O, Mg, Si, and Fe mean charge states in the CC segments and the preceding 24 hr of solar wind versus their corresponding mean carbon charge states in Figure 4. It is by construction that all the IC segments have mean charge state ratios $Q_{CC}/Q_{SW} < 1$, and the COC segments have $Q_{CC}/Q_{SW} > 1$ for all investigated elements: O, Mg, Si, and Fe. The two types are located on the top part and bottom part of the distribution, respectively. The IC segments tend to be carbon colder, but the difference between IC and COC segments may be mainly due to the outlier at $Q_C \approx 4.48$.

Thus, we performed a significance test on our classification of IC and COC type in the CC class. As we introduced previously, IC type was defined by its lower carbon mean charge and lower mean charge of O, Mg, Si, and Fe than the preceding solar wind, while COC type was defined by its lower carbon mean charge and higher mean charge of O, Mg, Si, and Fe. The tests are on the carbon ionic temperature and are performed to the three types of period: (1) CC, (2) IC, and (3) COC. Note that the CC type is the mother type, and IC type and COC type are two daughter types. Our null hypothesis is that the two distributions are the same. The test results are shown in Figure 5. The p values are 0.11, 0.43, and 0.06 for the three pairs: CC and IC, CC and COC, and IC and COC, respectively. Since we chose a significance level of 10%, the p-value less than 0.1 means the null hypothesis can be rejected at the 10% significance level. Clearly, the two daughter types are similar to their mother type (as seen by the p value of 0.11 and 0.43). However, the two daughter types, having a p value of 0.06, are very different. Indeed, as shown in Figure 5, the distributions of IC and COC cover different ionic temperature range and have little in common. These may suggest that these two types of cold material have different forming mechanisms.

Moreover, we investigated the relation between the ratios of average O, Mg, Si, and Fe average charge states to C average charge state and the bulk solar wind speed measured during CC

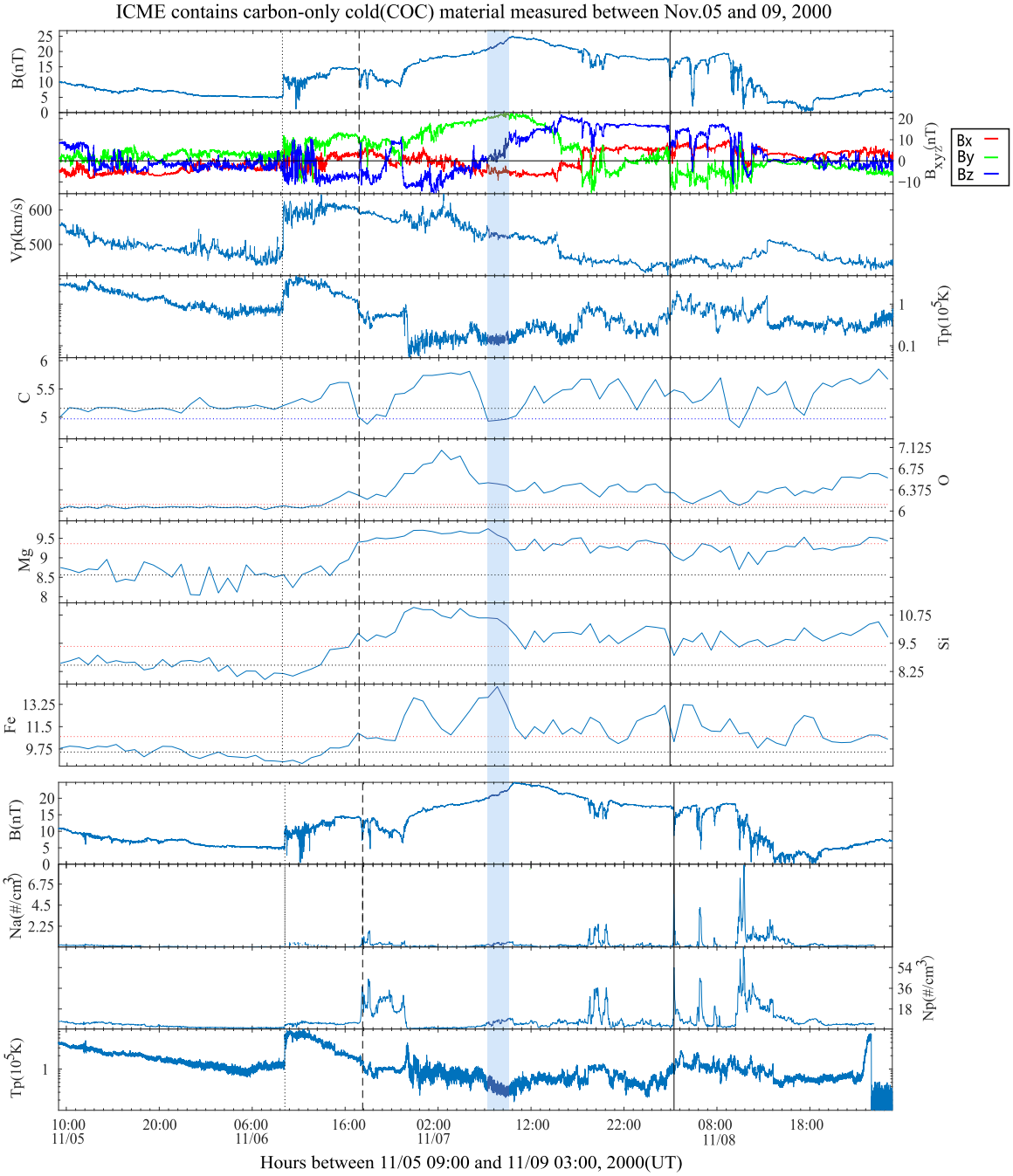

Figure 2. One ICME event containing carbon-only cold (COC) material. The top nine panels show the magnetic field magnitude, magnetic field components in GSE coordinates, proton speed, proton temperature, and mean charge state of C, O, Mg, Si, and Fe ions measured by *ACE*. The remaining four panels show the Wind measurements of the B, N_α, N_p, and T_p. The vertical black dotted line denotes the shock driven by the ICME. The vertical black dashed line denotes the start of the ICME. The vertical black solid line denotes the possible end of the ICME. The blue shaded stripe denotes the temporal segment when the cold material appeared. The black horizontal dashed line denotes the mean charge of the 24 hr of preceding solar wind. The horizontal red dotted line marks the $\langle Q\rangle_{\rm SW}+3\sigma_{Q\rm SW}$.

periods, and found no distinction between the IC and the COC types. Since O, Mg, Si, and Fe ions have the same variation trend in the IC and COC segments, we examined the correlation between the mean charge state of O and those of Mg, Si, and Fe ions. The results are shown in Figure 6. It is obvious that the mean charge of C is uncorrelated to that of O, shown in subgraph (a). From subgraph (b) and (c), we found very good correlations between the mean charge states of Mg (Si) ions to that of O ions for both types of segments. The subgraph (d) shows the mean charge states of Fe ions to that of O ions. The Fe–O correlation is less significant than the Mg (Si).

To further understand the nature of cold materials, we calculated the CME launch time $T_{\rm early}$ and $T_{\rm late}$ from the in situ measured ICME maximum and minimum velocities. The velocity information is given in the first appendix table. Considering the velocity variation during the CME initiation, we defined the CME start time range as [$T_{\rm early}-12$ hr, $T_{\rm late}+12$ hr]. According to this CME start time range, we checked the *SOHO* and *STEREO* CME lists. We identified all the CMEs having an angular width of

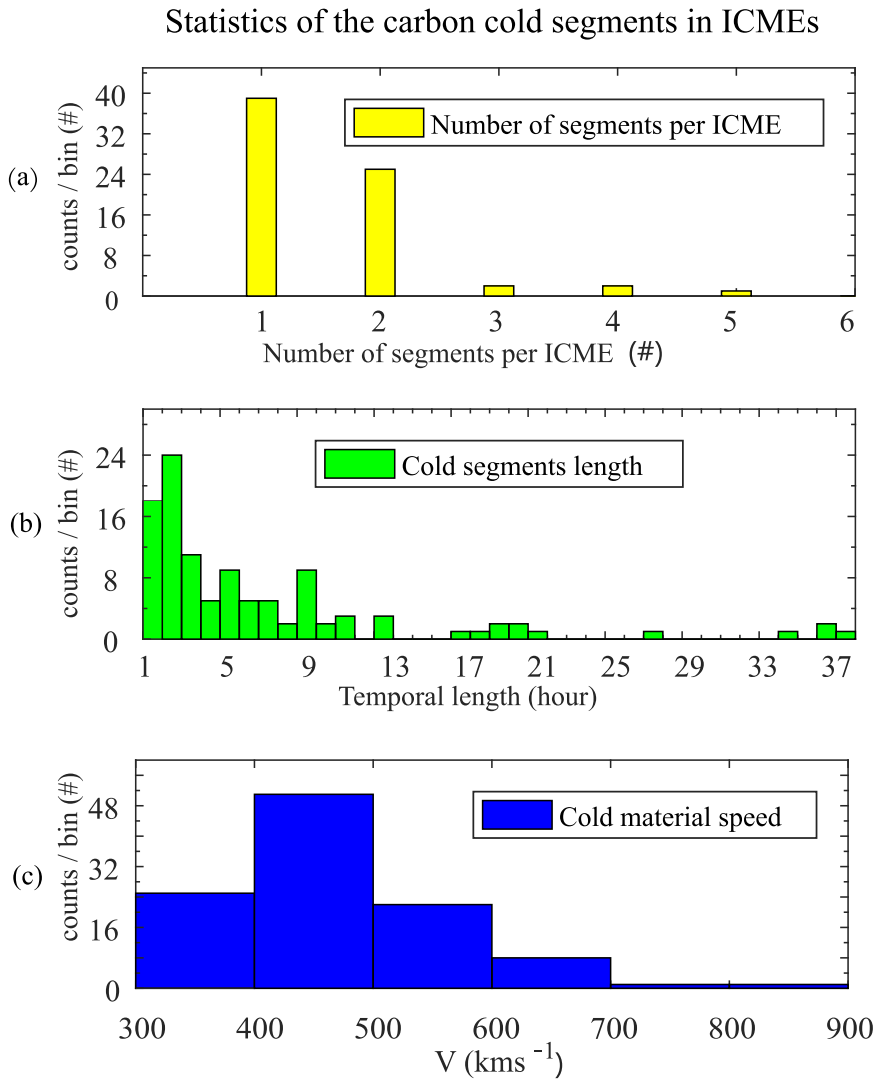

Figure 3. Distribution of the 108 carbon-cold segments in terms of (a) the number of segments per ICME, (b) the segment duration, and (c) the proton speed. The vertical axis in all three panels is the number of counts of the cold segments. In the top panel, the horizontal axis denotes the number of segments per ICME event. In the middle panel, the horizontal axis denotes the segment duration. In the bottom panel, the horizontal axis denotes the proton speed of each segment.

larger than 120° as Halo CMEs because Shen et al. (2014) reported that these CMEs have greater probability of hitting Earth and thus *ACE* and *WIND* than others. If there is more than one Halo CME in the start time range, we chose the Halo CME having the largest angular width. We identified the core part of the CMEs from 1998 February to 2005 August using UVCS on *SOHO* (-Giordano et al. 2013). For the CMEs occurring after 2007 April, we checked the observations from SECCHI and EUVI on *STEREO*. The CME counterparts of the 18 ICME events containing IC and COC materials are listed in Table 3. Because UVCS stopped working in 2005 September and *STEREO* only began observations in 2007 April, we could not determine whether CMEs had bright cores if they were observed between 2005 September and 2007 March. Thus, we marked them as unknown (U). The information of all the 69 CC ICMEs are shown in Table 8 in the Appendix. There are 54 ICMEs containing CC material related to Halo CMEs and 18 of these 54 CMEs have a bright core inside. It is interesting to note that all COC events occurred before 2006, and all but one of the IC events occurred after 2006. In Table 3, no data (ND) means no solar observations from *SOHO*/LASCO, and no report (NR) means *SOHO* LASCO and UVCS do not report such phenomenon though the data are available.

To reveal more features of the cold materials and to compare them with the filaments, we studied various plasma parameters of the cold materials. Thus, Table 3 also includes the T_p, N_p, N_α, and $R_{\alpha p}$ (N_α/N_p) for both IC and COC segments compared with their mean value of each ICME. The mean values of T_p, N_p, N_α, and $R_{\alpha p}$ in CC period and those in ICME are given in Table 8 in the Appendix. The comparison results of the three classes: CC, IC, and COC, are summarized in Table 4. It could be seen that the proton temperature for the IC segments and the COC segments have almost opposite trends. Furthermore, all cold materials tend to have higher $R_{\alpha p}$; and except IC segments, they tend to have lower proton temperatures as well.

Previously, Lepri & Zurbuchen (2010) reported the existence of cold filament materials in ICMEs. To define the cold filament materials, they used a combination of the charge states of the C, O, and Fe ions. Specifically, they defined the following: if $C^{2+,3+}$ represents more than 3.4% of all the measured carbon ions, O^{4+} represents more than 0.9% of all the measured oxygen ions, and $Fe^{4+,5+,6+,7+}$ represents more than 12.1% of all the measured iron ions, then the

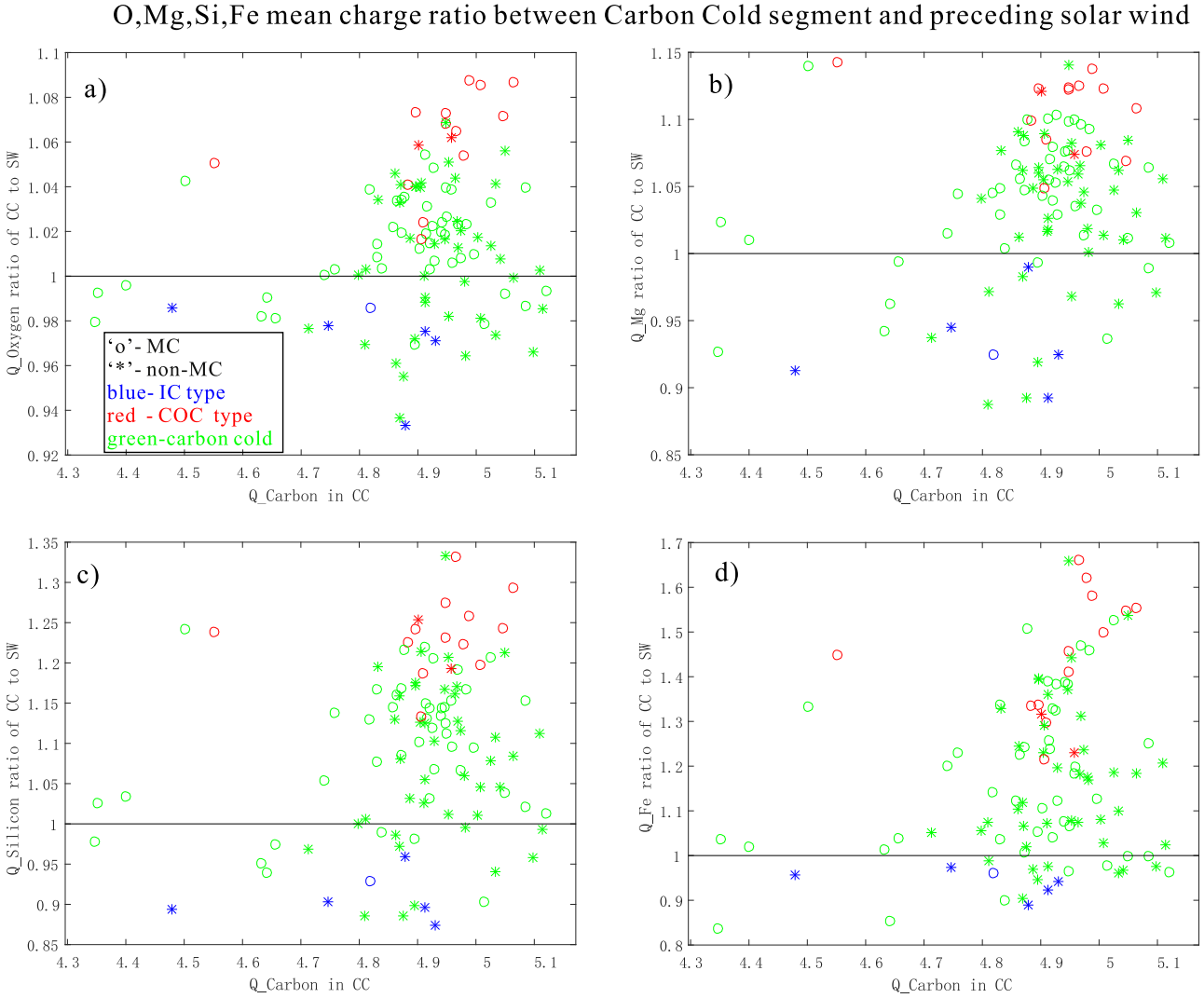

Figure 4. Distribution of the 108 carbon-cold segments in terms of the Q_{CC}/Q_{SW} of O, Mg, Si, and Fe ions in the four subgraphs (a), (b), (c), and (d) respectively. The vertical axis is the Q_{CC}/Q_{SW}. The horizontal axis is the mean charge state of C ions. The circle represents the cold segment occurring in MC, and the star means the cold segment occurring in Non-MC ICME. The IC segments are marked in blue, and the COC segments are marked in red. All the other cold segments are in green. The black solid line marks the ratio as 1.

corresponding plasmas are considered predominantly cold materials. In our study, we employed a different criterion for the identification of cold materials. Since the ICME events that we used in this study significantly overlap with Lepri & Zurbuchen (2010), we can compare our results with those studied by Lepri & Zurbuchen (2010). This comparison is presented in Table 5. A total of 11 cold filaments in 10 ICMEs were identified in Lepri & Zurbuchen (2010). The serial numbers of the 11 periods in Lepri & Zurbuchen (2010) and in our study are given in Table 5 as SN(L) and SN. Out of the 11 (Lepri & Zurbuchen 2010) cold material periods, 8 meet our definition of CC materials. Note that 3 of Lepri & Zurbuchen (2010) periods contain only a single data point for the carbon mean charge meeting the requirement on cold materials, marked by S. We noticed that 1 out of the 8 CC periods contains COC materials, and no periods contain IC materials. Note that the ICMEs reported by Lepri & Zurbuchen (2010) containing SN(L) 6, SN(L) 7, and SN(L) 9 cold material periods are not in our 219 ICME list, and are marked by "–" in Table 5. This is because our selection criteria require simultaneous measurements of ICMEs by both *ACE* and *WIND* as well as measurement of the solar wind within 24 hr prior to the ICMEs. For the ICMEs in Table 5, although the ICME events identified in both studies are the same, the duration of the segments differs, as they are identified by the two different criteria, as explained above. In addition, there are CMEs and filaments related to the SN(L) 4 and SN(L) 5 cold material periods in Lepri & Zurbuchen (2010). But in our study we found a Halo CME related to SN(L) 4 and no Halo CME related to SN(L) 5. Since we defined the range of CME start time using the in situ measured speed, we only checked the CME record in the defined time range. Beside, there is NR of eruptive prominence in the CME related to SN(L) 4 in our study.

Finally, we examined the solar cycle dependence of these cold material appearances. The results are shown in Figure 7. ICMEs are often classified into MCs and nonmagnetic-cloud ICMEs (non-MC). In our study, depending on if there are cold materials present, we further classified MC and non-MC into cold material ICMEs (CC ICMEs) and non-cold material ICMEs (non-CC ICMEs). Thus, a total of four types of ICMEs are shown in Figure 7. The blue bar indicates MCs with cold

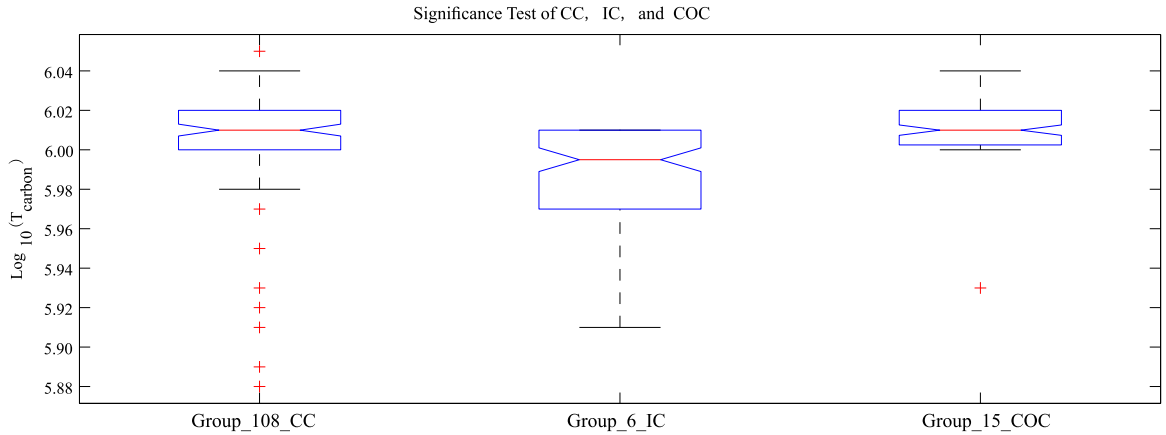

Figure 5. This figure shows the significance test on the carbon ionic temperature for three types of segments: carbon-cold segments, IC segments, and COC segments. The distributions of carbon ionic temperature for all three groups are assumed to be Gaussian. The *Y*-axis is the carbon ionic temperature in $\log_{10}$, and the *x*-axis shows the three groups. The horizontal red line marks the median of each group. The blue top and bottom edges of the box mark the first and third quantiles. Outliers are marked as red pluses. The black horizontal line marks the boundary between normal data and outliers.

Table 3
Plasma Moments of the Carbon-cold Materials in the ICMEs

SN	CC Start (YYYY/MM/DD UT)	CC End (YYYY/MM/DD UT)	T_p	N_α	N_p	$R_{\alpha p}$	Halo CME	Core	Type
53	2000 Jun 13 2312	2000 Jun 14 0431	H	H	H	H	Y	NR	IC
191	2006 Apr 14 0538	2006 Apr 14 1301	H	H	L	H	Y	U	IC
201	2009 Jan 19 0542	2009 Jan 19 1053	H	L	L	H	Y	Y	IC
213	2011 Feb 04 2044	2011 Feb 05 0420	H	H	L	H	Y	Y	IC
219	2011 Aug 07 0026	2011 Aug 07 0248	H	L	L	H	Y	Y	IC
219	2011 Aug 07 1824	2011 Aug 07 2014	L	H	H	L	Y	Y	IC
13	1998 Sep 25 1432	1998 Sep 25 1808	L	H	H	H	ND	ND	COC
17	1998 Nov 09 0408	1998 Nov 09 0633	L	H	H	H	Y	NR	COC
24	1999 Apr 16 2158	1999 Apr 17 1600	L	H	L	H	Y	NR	COC
31	1999 Jul 28 1947	1999 Jul 29 0130	L	H	H	L	Y	NR	COC
46	2000 Feb 21 1242	2000 Feb 21 1438	H	H	H	H	NR	NR	COC
46	2000 Feb 21 2110	2000 Feb 22 0027	L	H	L	H	NR	NR	COC
68	2000 Nov 07 0709	2000 Nov 07 0918	L	H	L	H	Y	Y	COC
82	2001 Apr 12 1030	2001 Apr 12 1151	L	H	H	L	Y	NR	COC
87	2001 Apr 29 0410	2001 Apr 29 1154	L	H	H	L	NR	NR	COC
120	2002 Mar 24 1442	2002 Mar 24 1654	L	H	L	H	Y	NR	COC
136	2002 Dec 18 0657	2002 Dec 18 0947	L	L	L	L	Y	NR	COC
149	2003 Nov 21 0209	2003 Nov 21 0354	L	H	L	H	Y	Y	COC
152	2004 Apr 04 1113	2004 Apr 04 2251	L	H	L	H	NR	NR	COC
152	2004 Apr 05 0043	2004 Apr 05 1102	L	H	L	H	NR	NR	COC
170	2005 May 15 1519	2005 May 15 1849	L	H	H	L	Y	Y	COC

Table 4
Moments of Carbon-cold Materials

Class	Segment Counts	T_p	N_p	N_α/N_p	In MC	Measured
IC	6	5 high	4 low	5 high	5 no	5 post 2006
COC	15	14 low	8 low	10 high	13 yes	15 pre 2006
CC	108	78 low	46 low	71 high	49 no	absent in 2008

materials, the orange bar indicates MCs without cold materials, the gray bar indicates non-MCs with cold materials, and the yellow bar indicates non-MCs without cold materials. Clearly, cold materials can appear in both MC and nonmagnetic-cloud ICMEs. Furthermore, the number of ICMEs containing cold materials represented by the blue and gray bars, is higher from 1998 to 2002 than from 2006 to 2011. The black and white cross symbols indicate the occurrence of ICMEs containing IC and COC materials, respectively. This suggests some solar activity dependence for the presence of cold materials. The fraction of MCs and CC ICMEs of each year are shown in panel (b) of Figure 7 as black and red solid lines, respectively. Uncertainties are included in these two plots. Assuming the uncertainty of the count is given by $\sqrt{N}$ (i.e., a Poissonian

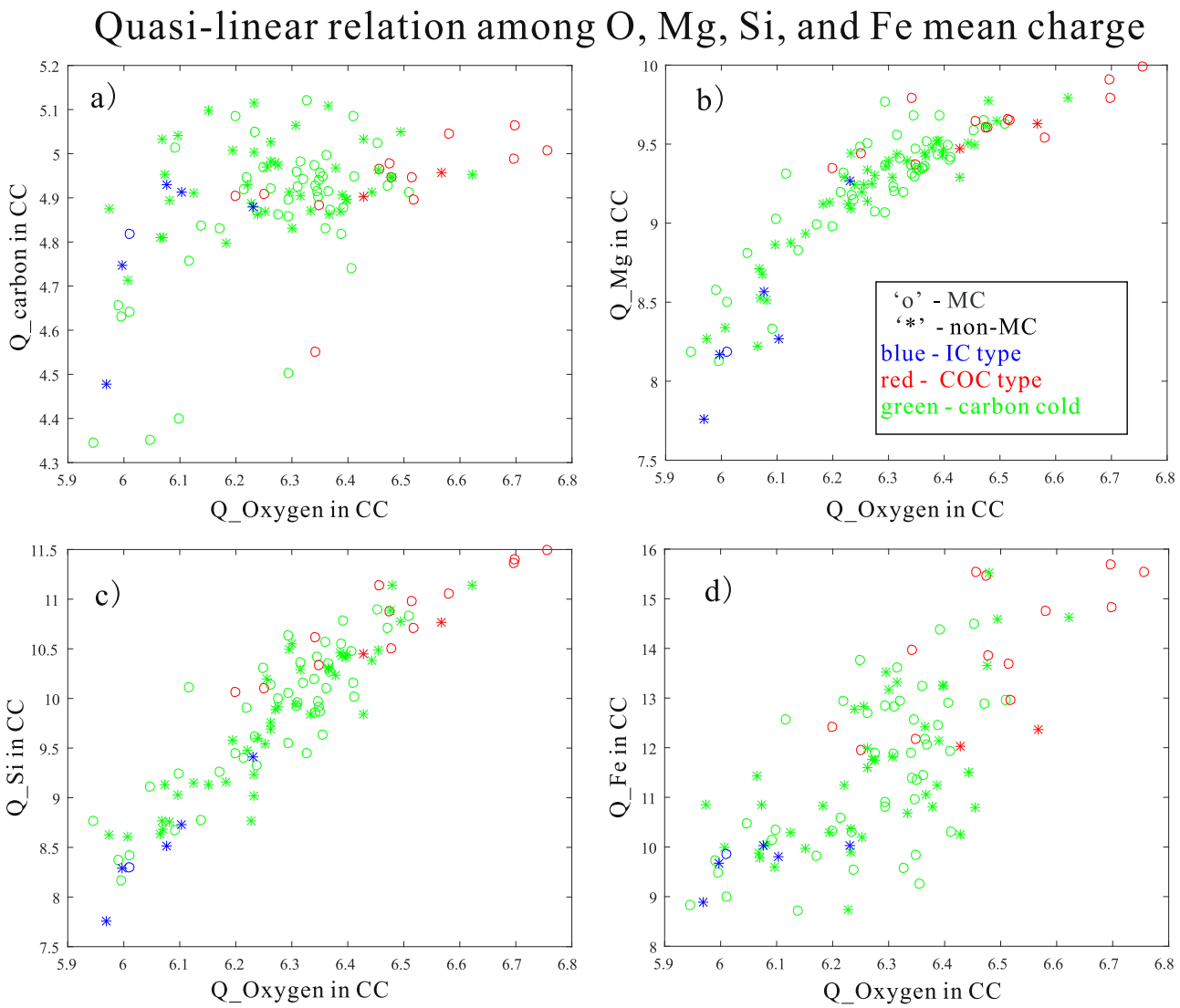

Figure 6. Distributions of the 108 carbon-cold segments in terms of the Q_C against Q_O, Q_{Mg} against Q_O, Q_{Si} against Q_O, and Q_{Fe} against Q_O are shown in the subgraph (a), (b), (c), and (d). The meaning of all symbols is the same as in Figure 4.

Table 5
Cold Filament Materials in the ICMEs

SN(L)	SN	Year	DOY UT	Date	ICME	MC	Filament(L)	Carbon-cold
1	5	1998	122 08:09–123 00:11	May 2	Yes	Yes	Yes	Yes
2	13	1998	268 10:04–268 12:04	Sep 25, 26	Yes	Yes	No LASCO CME	No
3	13	1998	269 08:16–269 12:17	Sep 25, 26	Yes	Yes	No LASCO CME	Yes
4	24	1999	107 04:10–107 10:12	Apr 17	Yes	Yes	Yes	Yes(COC)
5	46	2000	52 14:38–52 16:38	Feb 21	Yes	Yes	Yes	Yes(S)
6	–	2000	198 10:00–198 12:00	Jul 16	Yes	Yes	Yes	No
7	–	2001	295 08:55–295 11:58	Oct 22	Yes	No	Yes	Yes(S)
8	133	2002	253 03:53–253 09:53	Sep 10	Yes	Yes	Yes	No
9	–	2003	300 22:16–301 07:58	Oct 27	Yes	Yes	No	Yes
10	165	2005	9 07:59–9 19:59	Jan 9	Yes	Yes	Yes	Yes
11	171	2005	140 08:08–140 12:08	May 20	Yes	Yes	Yes	Yes(S)

distribution) for each category, the uncertainty of the ratio X/Y is calculated as

$$\delta^2(X/Y) = \frac{X}{Y^2} + \frac{X^2}{Y^3};$$

Y represents the yearly total number of ICMEs, and X represents the yearly total MC number and CC ICME number, for the two plots respectively. It could be seen that the fraction of CC ICMEs is less than or equal to that of MCs. Panel (c) shows yearly total

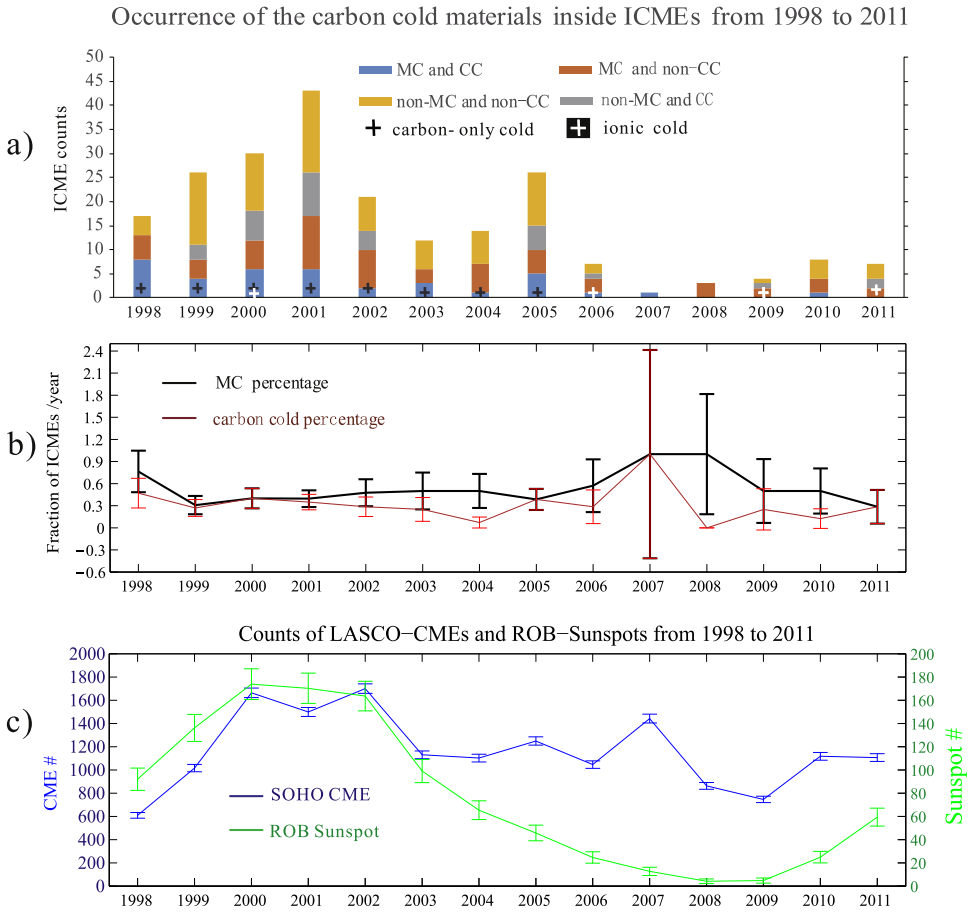

Figure 7. Yearly distribution of 219 studied ICMEs from 1998 to 2011. ICMEs are classified in four different types: magnetic cloud with cold material (MC and CC), magnetic cloud without cold material (MC and non-CC), nonmagnetic cloud with cold material (non-MC and CC), and nonmagnetic cloud without cold material (non-MC and non-CC). The horizontal axis is the year, which ranges from 1998 to 2011. The panel (a) shows the number of ICME events. In each year, the histogram of each of the four types of ICMEs is shown. In panel (b) the black line and the red line indicate the percentage of MCs and carbon-cold ICMEs, respectively. And panel (c) shows the yearly total CME number observed by *SOHO*/LASCO (left *Y*-axis) and the yearly mean sunspot number recorded by Royal Observatory of Belgium (right *Y*-axis).

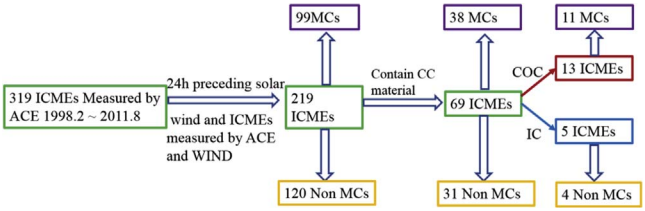

Figure 8. Quantitative information of ICMEs in this statistical study.

CME number observed by *SOHO*/LASCO and yearly averaged sunspot number recorded by the Royal Observatory of Belgium. It is obvious that the two plots have different variation trends. According to Wang & Colaninno (2014), the high CME number after mid-2010 is an artifact caused by identification of "very poor" eruptions and by LASCO image cadence. After calibration in Wang & Colaninno (2014), the *SOHO*/LASCO CME number shows a similar trend to sunspot number.

4. Discussion

In this study, we examined 219 ICME events detected by both the *ACE* and *WIND* spacecraft from 1998 to 2011. Using a criterion based solely on the average carbon charge state, we identified CC material in 69 of these ICMEs. Our results are summarized in the following text and in Figure 8. First, 69 of the 219 studied ICMEs contain cold material as defined by the criteria discussed in Section 2. Of these ICMEs, 38 are MCs. Only 18 out of 69 CC ICMEs can be confirmed to have clear three-part CME counterparts. Of these 18 events, 4 events have been previously reported by Lepri & Zurbuchen (2010). Second, the most probable duration of the segments during which the cold material is present is 2 hr, while approximately 80% of the segments last for less than 10 hr. The 69 CC ICMEs typically have one or two CC segments, rarely more than that. Third, the bulk solar wind proton speed for these segments typically lies between 300 and 600 km s^{-1}. In addition, segments containing cold materials tend to have a lower proton temperature, and higher $R_{\alpha p}$ comparing to their corresponding ICMEs. Fourth, we have identified two extreme populations for the periods that contain cold materials, one is the IC type and the other is the COC type. Ionic-cold type (6/108) has simultaneously lower average charge states of C, O, Mg, Si, and Fe than that of the 24 hr of solar wind preceding to the ICMEs (at 3σ-level). In comparison, COC type (15/108) has carbon being cold, but O, Mg, Si, and Fe are 3σ hotter than the preceding solar wind. We noticed that 11 of 13 ICMEs containing COC material are MCs, and 4 of 5 ICMEs containing IC material are non-MCs. To test if the appearance of COC and IC material in MC or non-MC is statistically

significant or not, we made the following hypothesis. We assumed that the COC were randomly distributed in all 219 studied ICMEs. Considering 99 of 219 ICMEs are MCs, so the probability that 11 of 13 ICMEs containing COC material are MCs is $C_{13}^{11}C_{206}^{88}/C_{219}^{99}= 0.003$. The very small probability means the null hypothesis should be rejected. Besides, we made Z-test on COC appearance ratios of the MC (11/99) and non-MC (2/120) groups, assuming the appearance probability of the two groups is the same. The Z value is 2.94 larger than the critical value for 95% confidence $Z_{0.05} = 1.645$. It means that the null hypothesis should be rejected. Thus, the COC material is not randomly distributed in 219 ICMEs, and its appearance in MCs has strong statistical significance. Next, we made the same hypothesis on IC material. The probability that 4 of 5 ICMEs containing IC material are non-MCs is 0.203, and the Z value is 1.14. It means the appearance of IC material may not be random, and its appearance in non-MCs is not very significant. We supposed that this weak result of IC is caused by the small number of IC samples.

We also noted that the IC material shows a higher proton temperature, and the COC material shows a lower proton temperature. Finally, there are four ICMEs containing cold material identified by both Lepri & Zurbuchen (2010) and our study. Only one of four, SN(L) 4 or SN 24, is classified as a COC type. This is due to the fact that the two temporal segments are slightly different.

Considering the above statistical features of the cold materials in the ICMEs, the relevant questions would be what is the nature of the cold material and how is it formed? Note that cold materials are not unique to ICMEs. A study by Zhao et al. (2017) reported that the decrease in the ratio of $\frac{C^{5+}/C^{6+}}{O^{6+}/O^{7+}}$ appears in approximately 10% of slow solar wind. In addition, the slow solar wind in that work was defined as having a speed of less than 500 km s^{-1}. They explained that the $\frac{C^{5+}/C^{6+}}{O^{6+}/O^{7+}}$ decreases as a result of either high-altitude reconnection heating or high-altitude wave particle interactions. The same phenomenon was also reported by Kocher et al. (2017) in the study of ICMEs. Checking our COC materials, we found all of them having lower $\frac{C^{5+}/C^{6+}}{O^{6+}/O^{7+}}$. In addition, the speed of our cold materials is typically less than 500 km s^{-1}.

For the COC materials related to the filaments, the mean charge difference between the carbon ions and other heavier ions may be related to the initiation process of the CMEs. It is known that the freeze-in heights of the C, O, Mg, Si, and Fe ions are different. For example, in the slow wind, the carbon ion charge state is the first to freeze-in at approximately 1.2 solar radii (R_s) (Geiss et al. 1995). Therefore, one possible process for forming COC type filament materials may be heating and collision beyond the carbon freeze-in height. During the eruption of CME, if the reconnection occurs above the carbon freeze-in height, but lower than those for other ions, then one expects that the carbon is cold, but other ions can go through ionizations and become hotter. Another possible explanation for the COC filament materials' formation is the prominence condensation in hot coronal loops. This has long been studied by Antiochos & Klimchuk (1991), Antiochos et al. (2000), and Karpen et al. (2005); it has been found that the filament material laying on the hot coronal loop is a combination of the cool condensed coronal plasmas and the evaporated chromospheric plasmas resulting from the pressure imbalance. Thus, the COC type filament materials may be a bulk of mixed ions from both the corona and the chromosphere.

It is not easy to understand the process leading to the formation of IC type filament materials. On one hand, the lower mean charges of all the C, O, Mg, Si, and Fe ions compared to that of the solar wind means that plasmas may not be sufficiently heated under 5 R_s (Geiss et al. 1995). On the other hand, the higher proton temperature means that the protons of the IC type filament materials tend to be heated. Such a heating may be possible by waves. It seems that in the events containing IC type filament materials the CMEs erupt without strong reconnection heating but are accompanied by preferential proton-wave resonance which efficiently heats protons. The fact that the IC type filament materials are found in non-MC ICMEs after the year 2006 and that the COC type filament materials are found in MCs before the year 2006, may suggest that these two types of filaments reflect fundamental differences between the two different solar cycles (Gopalswamy et al. 2015). Indeed, the solar activity was quite weak during the early years of the 24th solar cycle.

According to our study there are some IC and COC segments not related to the filaments. One possibility is that the core of CMEs were not observed due to the *SOHO* position and its instrument limitation. Another possibility is that these IC/COC segments do not correspond to filaments. As far as we know, there have been NRs of IC materials identified in the solar wind.

Our study suggests that there may be two different filament eruption processes, which have opposite effects on the ionization and proton temperatures. Although the occurrence rate of CC material in ICMEs is close to that of three-part CMEs, we cannot confirm that all CC segments are filament materials due to the limitation of solar observations before the *STEREO* era. Similar cold plasmas also appear in slow solar wind although with a lower occurrence rate (Zhao et al. 2017). Finally, we noted that further careful studies of IC materials may help us better understand both the CME initiation process and the heating mechanisms associated with the initiation. Such a study will benefit from the high-resolution imager on board the *Solar Dynamics Observatory* spacecraft (Pesnell et al. 2012) and future missions such as the Solar Orbiter (Mueller et al. 2013).

This work is supported by the Open Research Program of the Key Laboratory of Geospace Environment, Chinese Academy of Sciences (CAS), and by the Fundamental Research Funds for the Central Universities. The used ionization temperature is from CHIANTI database version 8. CHIANTI is a collaborative project involving George Mason University, the University of Michigan (USA) and the University of Cambridge (UK). All the *ACE* and *WIND* data is from NASA CDA web. The ICME list is originally from the *ACE* Science Center. The sunspot number is from Royal Observatory of Belgium. And the CME number is from CDAW Data Center. Dr. Yao and Mr. Feng thank Dr. Shen, C.L.; Dr. Wang, C.B.; Dr. Zhao, L.; and Dr. Song, H.Q. for their helpful discussions. The authors thank the referee for helpful questions and comments.

Appendix

This Appendix contains three supplemental tables. The full tables are available online. Here are some examples of them.

Table 6
The 219 ICMEs Measured by Both *ACE* and *WIND* between 1998 and 2011

SN	Shock YYYY/MM/DD UT	*ACE* Start	*ACE* End	V_{min} km s^{-1}	V_{max}	MC?
1	1998 Feb 17 0401	1998 Feb 17 0959	1998 Feb 17 2041	370	426	Yes
2	1998 Mar 04 1054	1998 Mar 04 1427	1998 Mar 06 0627	298	397	Yes
3	1998 Mar 30 2230	1998 Mar 31 1149	1998 Apr 03 0502	300	445	No
4	1998 Apr 11 1452	1998 Apr 12 0130	1998 Apr 13 1814	339	429	No
5	1998 May 01 2125	1998 May 02 0339	1998 May 04 0227	422	684	Yes

(This table is available in its entirety in machine-readable form.)

Table 7
Carbon Ionization Temperature of Carbon-cold Segments

SN	CC Start YYYY/MM/DD UT	CC End	Duration	V_{mean} km s^{-1}	log T_{CSW} K	log T_{CCC}
2	1998 Mar 04 1651	1998 Mar 06 0321	34^h30^m	338	6.09	6.00
2	1998 Mar 06 0426	1998 Mar 06 0627	2^h01^m	330	6.09	5.99
5	1998 May 02 1036	1998 May 03 2251	36^h15^m	510	6.09	5.89
8	1998 Jun 25 0414	1998 Jun 25 1528	11^h14^m	426	6.09	6.00
9	1998 Jun 26 0856	1998 Jun 26 1821	9^h25^m	466	6.09	6.00

(This table is available in its entirety in machine-readable form.)

Table 8
Plasma Moments of the Carbon-cold Materials in the ICMEs and the Related CMEs

SN	CC Start YYYY/MM/DD UT	CC End	T_p	N_α	N_p	$R_{\alpha p}$	Halo CME	Core	Type	T_{pICME} K	T_{pCC} K	$N_{\alpha ICME}$ cm^{-3}	$N_{\alpha CC}$ cm^{-3}	N_{pICME} cm^{-3}	N_{pCC} cm^{-3}	$R_{\alpha pICME}$	$R_{\alpha pCC}$
2	1998 Mar 04 1651	1998 Mar 06 0321	Low	High	Low	High	Yes	No Report		16761.68	16059.40	1.21	1.34	14.45	13.84	0.091	0.103
2	1998 Mar 06 0426	1998 Mar 06 0627	High	Low	High	Low	Yes	No Report		16761.68	26491.67	1.21	0.74	14.45	20.47	0.091	0.033
5	1998 May 02 1036	1998 May 03 2251	Low	High	Low	High	Yes	Yes		45476.01	27256.31	0.62	0.77	7.54	7.28	0.084	0.108
8	1998 Jun 25 0414	1998 Jun 25 1528	Low	High	High	High	Yes	No Report		35097.77	12819.25	0.86	1.31	14.93	15.97	0.054	0.080
9	1998 Jun 26 0856	1998 Jun 26 1821	Low	High	High	High	Yes	No Report		39699.19	23477.32	0.47	0.77	14.43	17.16	0.029	0.043
12	1998 Aug 20 1204	1998 Aug 20 2137	Low	High	Low	High	No data	No data		40123.10	25431.28	0.42	0.59	12.04	9.81	0.045	0.060
13	1998 Sep 25 1432	1998 Sep 25 1808	Low	High	High	High	No data	No data	COC	18219.73	11994.01	0.28	0.30	3.22	3.39	0.0870	0.0872

(This table is available in its entirety in machine-readable form.)

ORCID iDs

Gang Li https://orcid.org/0000-0003-4695-8866
Xiaoli Yan https://orcid.org/0000-0003-2891-6267

References

Antiochos, S. K., & Klimchuk, J. A. 1991, ApJ, 378, 372
Antiochos, S. K., MacNeice, P. J., & Speicer, D. S. 2000, ApJ, 536, 494
Aschwanden, M. J., Wuelser, J. P., Nitta, N. V., et al. 2009, SoPh, 256, 3
Burlaga, L., Fitzenreiter, R., Lepping, R., et al. 1998, JGR, 103, 277
Burlaga, L., Sittler, E., Mariani, F., et al. 1981, JGR, 86, 6673
Cane, H. V., & Richardson, I. G. 2003, JGRA, 108, 1156
Del Zanna, G., Dere, K. P., Young, P. R., et al. 2015, A&A, 582, A56
Dere, K. P., Brueckner, G. E., Howard, R. A., et al. 1997, SoPh, 175, 601
Forbes, T. G. 2000, JGR, 105, 23153
Geiss, J., Gloeckler, G., von Steiger, R., et al. 1995, Sci, 268, 1033
Giordano, S., Ciaravella, A., Raymond, J. C., et al. 2013, JGRA, 118, 967
Gloeckler, G., Cain, J., Ipavich, F. M., et al. 1998, SSRv, 86, 497
Gloeckler, G., Fisk, L. A., Hefti, S., et al. 1999, GeoRL, 26, 157
Gloeckler, G., & Geiss, J. 2007, SSRv, 130, 139
Gopalswamy, N. 2006, SSRv, 124, 145
Gopalswamy, N., Hanaoka, Y., Kosugi, T., et al. 1998, GeoRL, 25, 2485
Gopalswamy, N., Xie, H., Akiyama, S., et al. 2015, ApJL, 804, L23
Howard, T. A. 2015a, ApJ, 806, 175
Howard, T. A. 2015b, ApJ, 806, 176
Hudson, H. S., Bougeret, J.-L., & Burkepile, J. 2006, SSRv, 123, 13
Hundhausen, A. J., Sawyer, C. B., House, L., et al. 1984, JGR, 89, 2639
Karpen, J. T., Tanner, S. E. M., & Antiochos, S. K. 2005, ApJ, 635, 1319
Kasper, J. C., Stevens, M. L., Korreck, K. E., et al. 2012, ApJ, 745, 162
Kocher, M., Lepri, S. T., Landi, E., et al. 2017, ApJ, 834, 147
Landi, E., Oran, R., Lepri, S. T., et al. 2014, ApJ, 790, 111
Lepping, R. P., Acuna, M. H., Burlaga, L. F., et al. 1995, SSRv, 71, 207
Lepri, S. T., & Zurbuchen, T. H. 2010, ApJL, 723, L22
Lin, R. P., Anderson, K. A., Ashford, S., et al. 1995, SSRv, 71, 125
McCauley, P. I., Su, Y. N., Schanche, N., et al. 2015, SoPh, 290, 1703
McComas, D. J., Bame, S. J., Barker, P., et al. 1998, SSRv, 86, 563
Mueller, D., Marsden, R. G., St., Cyr, O. C., & Gilbert, H. R. 2013, SoPh, 285, 25
Ogilvie, K. W., Chornay, D. J., Fritzenreiter, R. J., et al. 1995, SSRv, 71, 55
Pesnell, W. D., Thompson, B. J., & Chamberlin, P. C. 2012, SoPh, 275, 3
Priest, E. R. 1988, Dynamics and Structures of Quiescent Solar Prominence (Berlin: Springer)
Reeves, K. K., McCauley, P. I., & Tian, H. 2015, ApJ, 807, 7
Richardson, I. G., & Cane, H. V. 2010, SoPh, 264, 189
Schwenn, R., Raymond, J. C., Alexander, D., et al. 2006, SSRv, 123, 127
Schwenn, R., Rosenbauer, H., & Muehlhaeuser, K.-H. 1980, GeoRL, 7, 201
Shen, C. L., Wang, Y. M., Pan, Z. H., et al. 2014, JGRA, 119, 5107
Smith, C. W., L'Heureux, J., Ness, N. F., et al. 1998, SSRv, 86, 613
Song, H. Q., Chen, Y., Li, B., et al. 2017, ApJL, 836, L11
Song, H. Q., Zhong, Z., Chen, Y., et al. 2016, ApJS, 224, 27
Wang, Y.-M., & Colaninno, R. 2014, ApJL, 784, L27
Wimmer-Schweingruber, R. F., Crooker, N. U., Balogh, A., et al. 2006, SSRv, 123, 177
Wood, B. E., Howard, R. A., & Linton, M. G. 2016, ApJ, 816, 67
Wurz, P., Ipavich, F. M., Galvin, A. B., et al. 1998, GeoRL, 25, 2557
Yan, X. L., Priest, E. R., Guo, Q. L., et al. 2016, ApJ, 832, 23
Yan, X. L., Qu, Z. Q., Kong, D. F., et al. 2013, A&A, 557, A108
Yao, S., Marsch, E., Tu, C.-Y., & Schwenn, R. 2010, JGR, 115, A05103
Zhao, L., Landi, E., Lepri, S. T., et al. 2017, ApJS, 228, 4
Zurbuchen, T. H., & Richardson, I. G. 2006, SSRv, 123, 31